New iron(II) cyclopentadienyl derivative complexes: Synthesis and antitumor activity against human leukemia cancer cells

Andreia Valente[a], Ana Margarida Santos[a], Leonor Côrte-Real[a], M. Paula Robalo[b,c], Virtudes Moreno[d], Mercè Font-Bardia[e, f], Teresa Calvet[e, f], Julia Lorenzo[g], M. Helena Garcia[a,*]

[a] Centro de Ciências Moleculares e Materiais, Faculdade de Ciências da Universidade de Lisboa, Campo Grande, 1749-016 Lisboa, Portugal
[b] Área Departamental de Engenharia Química, Instituto Superior de Engenharia de Lisboa, Rua Conselheiro Emídio Navarro, 1, 1959-007 Lisboa, Portugal
[c] Centro de Química Estrutural, Complexo I, Instituto Superior Técnico, Universidade de Lisboa, Av. Rovisco Pais, 1049-001 Lisboa, Portugal
[d] Department de Química Inorgànica, Universitat de Barcelona, Martí y Franquès 1-11, 08028 Barcelona, Spain
[e] Cristal.lografia, Mineralogia i Dipòsits Minerals, Universitat de Barcelona, Martí y Franquès s/n, 08028 Barcelona, Spain
[f] Centre Cientific i Tecnològic (CCiTUB), Universitat de Barcelona, Sole Sabaris 1-3, 08028 Barcelona, Spain
[g] Institut de Biotecnologia i de Biomedicina, Universitat Autònoma de Barcelona, 08193 Bellaterra, Barcelona, Spain

* Corresponding author.

E-mail address: lena.garcia@fc.ul.pt (M.H. Garcia).

ABSTRACT

A new family of "$Fe^{II}(\eta^5\text{-}C_5H_5)$" half sandwich compounds bearing a N-heteroaromatic ligand coordinated to the iron center by a nitrile functional group has been synthesized and fully characterized by NMR and UVeVis spectroscopy. X-ray analysis of single crystal was achieved for complexes 1 and 3, which crystallized in the monoclinic $P2_1/c$ and monoclinic $P2_1/n$ space groups, respectively. Studies of interaction of these five new complexes with plasmid pBR322 DNA by atomic force microscopy showed very strong and different types of interaction. Antiproliferative tests were examined on human leukemia cancer cells (HL-60) using the MTT assay, and the IC_{50} values revealed excellent antiproliferative activity compared to cisplatin.

1. Introduction

Organometallic chemistry emerged in the recent years as an attractive field for the search of new compounds as potential drugs for medicinal chemistry, in particular for chemotherapy. In this frame, metallocene derivatives have appeared at the end of the 1970s with the pioneering work of Köpf and Köpf-Maier involving the antitumor activity of early transition-metal cyclopentadienyl complexes [1]. The promising results obtained for dichloride metallocenes (Cp_2MCl_2, where M = Ti, V, Nb, Mo; Cp = η^5-cyclopentadienyl) showing antitumor activity against numerous tumors, such as Ehrlich ascites tumor, B16 melanoma, colon 38 carcinoma and Lewis lung carcinoma, as well as against several human tumors heterotransplanted to athymic mice, certainly constitute an important impulsion for the interest of this area [2]. Titanium dichloride, (η^5-C_5H_5)$2TiCl_2$, was the first of such species in clinical trials [3]. Nevertheless, problems related with formulation led to the abandonment of titanocene dichloride in Phase II clinical trials [4 -6]. Ferrocene derivatives also appeared with promising results showing activity against Rauscher leukemia virus and EAT in CF1 mice [7,8] and in P388 leukemia cells [9] reinoculated tumors [10]. Particularly, the ferrocifens family, which is a ferrocene derivative of tamoxifen (Astra Zeneca, London, UK e the drug used for treating breast cancer), has revealed good cytotoxicity activities. However, these molecules suffer from poor bioavailability restricting them from entering clinical trials. In order to overcome this limitation and advance toward clinical studies, several formulations are being tested, such as nanoparticles, lipid nanocapsules and cyclodextrins [11].

The half-sandwich family of compounds emerged more recently using different central metals and has revealed potentialities as anticancer drugs. The particular geometry of piano stool compounds provides a good scaffold for building new molecules by changing the coordinated arene, which can be η^6 or η^5-bonded, the chelated active ligand and also the coligands. In this context, [Ru(η^6-arene)(X)(Y-Z)] complexes (where Y-Z is a chelating ligand, and X is monoanionic ligand) revealed high cytotoxicity against human ovarian tumor cells [12 -15] and they are thought to act through covalent Ru-DNA interactions [16,17]. Related compounds incorporating the 1,3,5-triaza-7-phosphaadamantane (PTA) ligand, such as [Ru(η^6-p-cymene)(PTA)Cl2] (RAPTA-C), have shown activity against metastases and although their mechanism of action has not been established, a pH dependent interaction with DNA may be a key component [18]. During the last years, our research group has been exploring a third family of half-sandwich compounds based on the "$Ru^{II}(\eta^5\text{-}C_5H_5)$" fragment, with the general formula [Ru(η^5-Cp)(P-P)(L)][X] (where P-P is a chelating phosphane or two phosphane ligands, L is a N-heteroaromatic sigma ligand mono or bidentate ligand and X is a counterion) [19 - 24]. Our studies showed significant toxicity for a variety of cancer cell lines, namely LoVo and HT29 human colon adenocarcinoma, MiaPaCa pancreatic cancer cell lines, HL-60 human leukemia cancer cells, A2780 human ovarian cancer cells (and the resistant form A2780CisR), MCF7 and MDAMB231 human breast cancer cells (estrogen dependent and independent, respectively) and PC3 human prostate cancer cells, with IC_{50} values lower than those of cisplatin in most cases [19 -24]. One important advantage of

ruthenium based compounds for therapeutic uses compared to other metal complexes, is pointed out on its ability to mimic iron in binding biologically relevant molecules such as albumin and transferrin and consequently to show much lower toxicity than that of platinum therapies [25]. The success of the coordination of N-heteroaromatic ligands to the fragment 'RuCp' in terms of finding new compounds with important cytotoxicity against several cancer cell lines led us to extend our studies to the analog 'FeCp' derivatives. In this context, we have recently published our first results concerning a new family of compounds with the general cationic structure $[Fe(\eta^5\text{-}Cp)(P\text{-}P)(L)]^+$, where L is coordinated to the iron center by the N atom of the heteroaromatic ligand [26]. These new compounds showed values of cytotoxicity against MCF7 and HeLa much lower than the ones found for cisplatin in the same experimental conditions.

Having in mind to exploit the effect of cytotoxicity of other ligands coordinated by a different group than a N-heteroaromatic atom, we had previously studied two new $[Ru(\eta^5\text{-}Cp)(PPh_3)_2(N \equiv CL)]^+$ derived compounds where N ≡ CL was coordinated by a nitrile functional group (benzo[1,2-b; 4,3-b'] dithio-phen-2-carbonitrile and [5-(2-thiophen-2-yl)-vinyl]-thiophene-2-carbonitrile]) which were tested against HL-60 cells [20]. The IC_{50} values obtained after 24 h of incubation were 1.46 ± 0.25 and 5.89 ± 0.67 mM, respectively, while cisplatin in the same experimental conditions presented a higher IC_{50} value of 15.61 ± 1.15 mM. These motivating results obtained with ruthenium coordinated nitrile ligands together with our interest

to continue the exploitation of the cytotoxic properties of 'FeCp' compounds led us to the synthesis of a new family of iron nitrile compounds of general formula $[Fe(\eta^5\text{-Cp})(NCL)(P\text{-}P)]^+$. In the present paper we report the synthesis of compounds of the general formula $[Fe(\eta^5\text{-Cp})(NCL)(P\text{-}P)]^+$, where the NCL ligands, 2-quinolinecarbonitrile (L1), 3-quinolinecarbonitrile (L2), 2-pyrazinecarbonitrile (L3) or 2,3-pyrazinedicarbonitrile (L4), present on their structures one or two N-heteroaromatic rings. These new compounds were fully characterized and their interaction with plasmid pBR322 DNA was studied by atomic force microscopy. Moreover, their potentialities as cytotoxic agents against human leukemia cancer cells (HL-60 cells) were evaluated. Remarkably, our studied compounds revealed IC_{50} values lower than those of cisplatin. Apoptotic behavior was also evaluated and compared with cisplatin.

2. Experimental

2.1. General procedures

All syntheses were carried out under dinitrogen atmosphere using current Schlenk techniques and the solvents used were dried using standard methods [27]. $[Fe(\eta^5\text{-}C_5H_5)(dppe)I]$ was prepared following the method described in literature [28]. FT-IR spectra were recorded in a Mattson Satellite FTIR spectrophotometer with KBr pellets; only significant bands are cited in text. ^1H, ^{13}C and ^{31}P NMR spectra were recorded on a Bruker Avance 400 spectrometer at probe temperature. The ^1H and ^{13}C chemical shifts are reported in parts per million (ppm) downfield from internal Me_4Si and the ^{31}P NMR spectra are reported in ppm downfield from external standard, 85% H_3PO_4. Elemental analyses were obtained at Centro de Apoio Científico Tecnológico Á Investigación (C.A.C.T.I.), at Universidade de Vigo, using a Fisons Instruments EA1108 system. Electronic spectra were recorded at room temperature on a Jasco V-560 spectrometer in the range of 200-900 nm.

2.2. Complexes synthesis

2.2.1. General procedure applied to the synthesis of the complexes 1-5

To a stirred suspension of 0.5 mmol of [FeCp(dppe)I] in dichloromethane (25 mL) was added 0.6 mmol of the adequate ligand (L1 = 2-quinolinecarbonitrile; L2 = 3-quinolinecarbonitrile; L3 ¼ 2-pyrazinecarbonitrile; L4 = 2,3-pyrazinedicarbonitrile) followed by addition of 0.6 mmol of $TlPF_6$ (for

complexes 1, 2, 3 and 4) or $AgCF_3SO_3$ (for complex 3). After refluxing for a period of 5-6 h the color changed from gray to orange reddish. The reaction mixture was cooled down to room temperature and the solution was filtered to eliminate the TlCl or the AgCl precipitate. The solvent was then removed under vacuum and the residue was washed with n-hexane (2 x 10 mL). Dark red crystals were obtained after recrystalization from dichloromethane/n-hexane solutions.

Compound 5 was obtained by stirring for 90 min, a suspension of 0.32 g (0.5 mmol) of [FeCp(dppe)I] and $TlPF_6$ (0.21 g, 0.6 mmol), in dichloromethane (25 mL) to which a solution of 2,3-dicianopyrazine in dichloromethane (0.078 g; 0.6 mmol) was slowly added. The obtained purple solution was dried and washed with n-hexane, giving a powder, which after recrystalization from dichloromethane/n-hexane, gave needle shaped purple crystals.

2.2.2. [FeCp(dppe)(2-cq)][PF6], 1

Dark red; Yield = 81%. IR (KBr, cm^{-1}): ν(C ≡ N, stretch) 2208, ν(PF_6) 837 and 557. ^{1}H NMR ($(CD_3)_2CO$, Me_4Si, *δ*/ppm): 8.30 (d, 1, H_{10}); 8.15 (t, 4, dppe); 7.96 (dd, 2, H_4 þ H_7); 7.88 (t, 1, H_6); 7.73 (t, 1, H_5); 7.53 (m,16, dppe); 6.78 (d,1, H_9) 4.75 (s, 5, h^5-C_5H_5); 2.80 (m, 4, CH_2-dppe). ^{13}C NMR ($(CD_3)_2CO$, Me_4Si, *δ*/ppm): 148.3 (C_8); 138.0 (C_9); 137.6-137.0 (C_q, dppe); 133.8 (CH-, dppe); 133.1 (C ≡ N); 132.5 (CH-, dppe); 132.2 (C_6); 131.6-131.4 (CH-, dppe); 130.3 (C_5); 130.0 (C_4); 129.9 (CH-, dppe + C_3); 129.4 (C_2); 128.9 (C_7); 123.8 (C_{10}); 81.4 (Cp); 28.4 (-CH_2-, dppe). ^{31}P($(CD_3)_2CO$, d/ppm): 96.2 (s, dppe); -144.2 (setp, PF_6). UV-Vis. in CH_2Cl_2, λ_{max}/nm (ε/M^{-1} cm^{-1}): 240 (73,195), 385 (6049), 441 (6893). UV-Vis. In DMSO, λ_{max}/nm (ε/M^{-1} cm^{-1}): 392 (Sh), 455 (7669). Elemental analysis (%) Found: C, 59.50; H, 4.30; N, 3.40; Calc. for $C_{41}H_{35}N_2P_3F_6Fe \cdot 0.1CH_2Cl_2$ (826.9): C, 59.70.16; H, 4.30; N, 3.40.

2.2.3. [FeCp(dppe)(3-cq)][PF6], 2

Dark red; Yield: 80%. IR (KBr, cm^{-1}): ν(C ≡ N, stretch) 2210, ν(PF_6) 837 and 557. ^{1}H RMN ($(CD_3)_2CO$, Me_4Si, *δ*/ppm): 8.15 (t, 4, C_6H_5-dppe); 8.00 (d, 1, H_5); 7.92 (m, 2, H_3 + H_7); 7.85 (d, 1, H_8); 7.71 (t, 1, H_6); 7.68 (s, 1, H_{10}); 7.58 (m, 16, C_6H_5-dppe); 4.73 (s, 5, η_5-C_5H_5); 2.82 (m, 4, CH_2). 13C NMR ($(CD_3)_2CO$, Me_4Si, *δ*/ppm): 149.9 (C_3); 148.8 (C_2); 142.3 (C_{10}); 137.7 - 137.1 (Cq, dppe); 134.0 (CH-, dppe); 133.8 (C_7); 132.4 (CH-, dppe); 131.7 - 131.4 (CH-, dppe); 130.1 (C_5); 130.0 (CH-, dppe); 129.4 (C_8); 129.3 (C_6); 126.5 (C_4); 107.1 (C_9); 81.1 (Cp); 28.5 (-CH2-, dppe); C_1 is overlapped by dppe signals. ^{31}P RMN ($(CD_3)_2CO$, *δ*/ppm): 97.1 (s, dppe); -144.2 (setp, PF_6). UV - Vis in CH_2Cl_2, λmax/nm (ε/M^{-1} cm^{-1}): 239 (75,639), 376 (7169), 429 (5136). UV - Vis in DMSO, λ_{max}/nm (ε/M^{-1} cm^{-1}): 386 (6559), 442 (7292). Elemental analysis (%) Found: C, 59.10; H, 4.30; N, 3.40; $C_{41}H_{35}N_2P_3F_6Fe$ (826.9): C, 59.2; H, 4.30; N, 3.30.

2.2.4. [FeCp(dppe)(3-cq)][CF_3 SO_3], 3

Dark red; Yield: 80%. IR (KBr, cm^{-1}): n(C ≡ N, stretch) 2212, $\nu(CF_3SO_3)$ 1269. ^{1}H NMR ($(CD_3)_2CO$, Me_4Si, δ/ppm): 8.15 (t, 4, C_6H_5-dppe); 8.01 (d, 1, H_5); 7.92 (m, 2, H_3 + H_7); 7.87 (d, 1, H_8); 7.71 (m, 2, H_{10} + H_6); 7.63 (t, 4, C_6H_5-dppe); 7.57 (m, 12, C_6H_5-dppe); 4.74 (s, 5, η^5-C_5H_5); 2.80 (m, 4, CH_2). ^{13}C NMR ($(CD_3)_2CO$, Me_4Si, δ/ppm): 149.7 (C_3); 148.6 (C_2); 142.6 (C_{10}); 137.7 -137.4 (Cq, dppe); 134.0 (CH-, dppe); 133.8 (C_7); 132.4 (CH-, dppe); 132.1 (C_1); 131.7 - 131.4 (CH-, dppe); 130.2 (C_5); 130.0 (CH-, dppe); 129.4 (C_8); 129.3 (C_6); 126.6 (C_4); 107.1 (C_9); 81.1 (Cp); 28.5 (-CH_2-, dppe). ^{31}P RMN (CD_3Cl_3, δ/ppm): 97.1 (s, dppe). UV - Vis in CH_2Cl_2, λ_{max}/nm (ε/M^{-1} cm^{-1}): 239 (51,562), 369 (3559), 428 (2371). UV - Vis in DMSO, λ_{max}/nm (ε/M^{-1} cm-^{1}): 386 (4380), 442 (4798). Elemental analysis (%) Found: C, 57.4; H 4.2; N, 3.08; $C_{42}H_{37}N_2P_2F_3SO_3$-Fe · CH_2Cl_2: C, 56.8; H, 4.32; N, 3.08.

2.2.5. [FeCp(dppe)(cpz)][PF_6], 4

Red; Yield: 85%. IR (KBr, cm^{-1}): n(C≡N, stretch) 2218, $\nu(PF_6)$ 837 and 557. ^{1}H NMR ($(CD_3)_2CO$, Me_4Si, δ/ppm) 8.67 (d, 1, H_4); 8.55 (d, 1, H_5), 8.05 (m, 4, C_6H_5), 7.88 (s, 1, H_3), 7.56 - 7.48 (m, 16, C_6H_5), 4.75 (s, 5, η^5-C_5H_5); 2.79 (m, 4, CH_2). ^{13}C NMR ($(CD_3)_2CO$, Me_4Si, δ/ppm): 148.9 (C3), 147.8 (C4), 146.2 (C5), 137.4 - 137.0 (Cq, dppe); 133.8 (CH-, dppe); 132.5 (CH-, dppe); 131.5 (CH-, dppe); 130.0 (CH-, dppe); 81.7 (Cp); 28.4 (-CH_2-, dppe).^{31}P NMR ($(CD_3)_2CO$, δ/ppm): 96.10 (s, dppe); -144.2 (setp, PF_6). UV-Vis in CH_2Cl_2, λ_{max}/nm (ε/M^{-1} cm^{-1}): 264 (20,282), 388 (2564), 445 (2895). UV-Vis in DMSO, λ_{max}/nm (ε/M^{-1} cm^{-1}): 446 (5225). Elemental analysis (%) Found: C, 55.75; H, 4.1; N, 5.35; Calc. for $C_{36}H_{32}N_3P_3F_6Fe$ · 1/10CH_2Cl_2: C, 55.74; H, 4.17; N, 5.40.

2.2.6. [FeCp(dppe)(2,3-dcpz)][PF_6], 5

Purple; yield: 86%. IR (KBr, cm^{-1}): n(C≡N, stretch) 2198, n(PF_6) 837 and 559. ^{1}H RMN ($CDCl_3$, Me_4Si, δ/ppm): 8.84-8.81 (m, 2, H_4 + H_5); 8.00 (t, 4, C_6H_5); 7.48 (m, 16, C_6H_5); 4.86 (s, 5, η^5-C_5H_5); 2.85 (m, 4, CH_2). ^{13}C NMR ($(CD_3)_2CO$, Me_4Si, δ/ppm): 148.8 (C_4); 147.0 (C_5); 137.1-136.6 (Cq, dppe); 133.8 (CH-, dppe); 133.2 (C_2 + C_3); 131.7 (CH-, dppe); 130.1 (CH-, dppe); 120.0 (CH-, dppe); 128.7 (C_1); 114.6 (C_6); 82.7 (Cp); 28.6 (-CH2-, dppe). ^{31}P RMN ($(CD_3)_2CO$, δ/ppm): 95.4 (s, dppe); -144.27 (setp, PF_6). UV- Vis in CH_2Cl_2, λ_{max}/nm (ε/M^{-1} cm^{-1}): 266 (12,201), 521 (2521). UV-Vis in DMSO, λmax/nm (ε/M^{-1} cm^{-1}): 512 (5710). Elemental analysis (%) Found: C, 55.10; H, 4.0; N, 6.90; Calc. for $C_{41}H_{35}N_2P_3F_6Fe$ · 0.2CH_2Cl_2 (811.40): C, 55.94; H, 3.93; N, 7.05.

2.3. Crystal structure determination of [FeCp(dppe)(2-cq)][PF_6] 1 and [FeCp(dppe)(3-cq)][CF_3SO_3] 3

Prismatic crystals (0.1 x 0.1 x 0.2 mm and 0.2 x 0.1 x 0.1 mm respectively) were selected and mounted on a MAR345 diffractometer with an image plate detector. Intensities were collected with graphite monochromatized Mo Kα radiation. Lorentzpolarization and absorption corrections were made. The structures were solved by Direct methods, using SHELXS computer program [29] and refined by full-

matrix least-squares method with SHELX93 computer program [30], (very negative intensities were not assumed). The function minimized was $\Sigma w||Fo|^2 - |Fc|^2|^2$, where $\omega = [\sigma^2(I) + (0.0566P)^2 + 0.4472P]^{-1}$, and $P = (|Fo|^2 + 2|Fc|^2)/ 3$, *f*, *f*' and *f*" were taken from International Tables of X-Ray Crystallography [31]. All H atoms were located from a difference synthesis and refined with an overall isotropic temperature factor. CCDC 939633 and 939634 contain the supplementary crystallographic data for this paper. These data can be obtained free of charge from the Cambridge Crystallographic Data Centre via www. ccdc.cam.ac.uk/data_request/cif.

2.4. Electrochemical experiments

The electrochemical experiments were performed on an EG&G Princeton Applied Research Model 273A potentiostat/galvanostat and monitored with a personal computer loaded with Electrochemistry PowerSuite v2.51 software from Princeton Applied Research. Cyclic voltammograms were obtained in 0.1 M or 0.2 M solutions of $[NBu_4][PF_6]$ in CH_3CN or CH_2Cl_2 respectively, using a three-electrode configuration cell with a platinum-disk working electrode (1.0 mm diameter) probed by a Luggin capillary connected to a silver-wire pseudo-reference electrode and a Pt wire counter electrode. The electrochemical experiments were performed under a dinitrogen atmosphere at room temperature. The redox potentials were measured in the presence of ferrocene as the internal standard and the redox potential values are normally quoted relative to the SCE by using the ferrocenium/ferrocene redox couple ($E_{1/2}$ = 0.46 or 0.40 V vs. SCE for CH_2Cl_2 or CH_3CN, respectively) [32]. The supporting electrolyte was purchased from Fluka, electrochemical grade was dried under vacuum for several hours and used without further purification. Reagent grade acetonitrile and dichloromethane were dried over P_2O_5 and CaH_2, respectively, and distilled under dinitrogen atmosphere before use.

2.5. DNA interaction studies

2.5.1. Formation of drugeDNA complexes

Deionized Milli-Q water (18.2 MΩ) was filtered through 0.2-nm FP030/3 filters (Schleicher & Schuell) and centrifuged at 4.000 g prior to use. pBR322 DNA was heated at 60 °C for 10 min to obtain open circular (OC) form. To stock aqueous solutions of plasmid pBR322 DNA in Hepes buffer (4 mM Hepes, pH 7.4/2 mM $MgCl_2$) were added aqueous solutions (with 4% of DMSO) of complexes 1-5 in a relationship DNA base pair to complex 10:1. In parallel experiments, blank sample of free DNA and DNA complex solutions were equilibrated at 37 °C for 4 h in the dark shortly thereafter.

2.5.2. AFM imaging

Atomic force microscopy (AFM) samples were prepared by casting a 3-μL drop of test solution onto freshly cleaved green mica disks as support. The drop was allowed to stand undisturbed for 3 min to favor the adsorbate-substrate interaction. Each DNA-laden disk was rinsed with Milli-Q water and was blown dry with clean compressed argon gas directed normal to the disk surface. Samples were stored over silica prior to AFM imaging. All AFM observations were made with a Nanoscope III Multimode AFM (Digital Instrumentals, Santa Barbara, CA). Nano-crystalline Si cantilevers of 125-nm length with a spring constant of 50 N/m average ended with conical-shaped Si probe tips of 10-nm apical radius and cone angle of 35° were used. High-resolution topographic AFM images were performed in air at room temperature (relative humidity < 40%) on different specimen areas of 2 x 2 mm operating in intermittent contact mode at a rate of 1-3 Hz.

296 *2.6. Growth inhibition assays*

297 Antiproliferative activity of these new iron complexes, and cisplatin, was tested in a cell culture system
298 using the human acute promyelocytic leukemia cell line HL-60 (American Type Culture Collection
299 (ATCC)). The cells were grown in RPMI-1640 medium supplemented with 10% (v/v) heat inactivated
300 fetal bovine serum, 2 mmol/L glutamine (Invitrogen, Inc.) in a highly humidified atmosphere of 95%
301 air with 5% CO_2 at 37 °C. Growth inhibitory effect was measured by the microculture tetrazolium [3-
302 (4,5- dimethylthiazol-2-yl)-2,5-diphenyltetrazolium bromide, MTT assay [33]. Cells were seeded at
303 density 104 cells/well in 100 mL of culture medium and after that cells were treated with different
304 concentrations ranging from 0 (culture medium) to 200 μM of compounds in 100 μl of culture medium.
305 The exact concentrations assayed were 0.1, 0.24, 0.5, 0.75, 1, 2.5, 5, 10, 25, 50, 100 and 200 μM. All
306 the assays were done in quadruplicate and three independent assays were realized. After incubation at
307 37 °C during 24 h or 72 h, without washing, 20 μl of soluble tetrazolium salt was added to each well
308 and incubated 3 additional hours. As we used soluble tretrazolium salts we determined the amount of
309 formazan directly reading the absorbance at 490 nm in a spectrophotometric plate reader (Labsystems
310 iEMS Reader MF). Cytotoxicity was evaluated in terms of cell growth inhibition in treated cultures
311 versus that in untreated controls. IC_{50}, the concentration of compound at which cell proliferationwas
312 50% of that observed in control cultures, were obtained by GraphPad Prism software, version 4.0.
313 Experiments were repeated at least three times to get the mean values.

314

315

316 *2.7. Apoptosis assays*

317 Induction of apoptosis in vitro by iron compounds was determined by a flow cytometric assay with
318 Annexin V-FITC by usingan Annexin V-FITC Apoptosis Detection Kit (Roche) [34]. Exponentially
319 growing HL-60 cells in 6-well plates (5×10^5 cells/well) were exposed to concentrations equal to the
320 IC_{50} of the platinum and iron drugs for 24 h. After, the cells were subjected to staining with the Annexin
321 V-FITC and propidiumiodide. The amount of apoptotic cells was analyzed by flow cytometry (BD
322 FACSCalibur).

323

3. Results and discussion

3.1. Synthesis of Fe(II) complexes

Five new cationic iron(II) complexes (1e5) of the general type [Fe(η^5-C_5H_5)(dppe)L][X] where L = 2-quinolinecarbonitrile (L1), 3-quinolinecarbonitrile (L2), 2-pyrazinecarbonitrile (L3) or 2,3-pyrazinedicarbonitrile (L4) and X = PF_6 or CF_3SO_3 were prepared by σ coordination of the functional nitrile N≡C group of the L1-L4 ligands (Scheme 1). Compounds were obtained in good yields (80-86%), by halide abstraction from [Fe(η^5-C_5H_5)(dppe)I] with thallium hexafluorophosphate or silver triflate, in dichloromethane, in the presence of a slight excess of the adequate ligand and recrystallized from dichloromethane/n-hexane solutions. The new compounds are stable in cellular media for several hours (Fig. S1, in SI) and were all fully characterized by FT-IR, ^{1}H, ^{13}C and ^{31}P NMR spectroscopies; the elemental analyses were in accordance with the proposed formulations. The structures of compounds 1 and 3 were also characterized by X-ray diffraction studies (see below).

Solid state FT-IR spectra (KBr pellets) of the complexes present the characteristic bands of the cyclopentadienyl ligand (≈3050 cm^{-1}), the PF_6 (840 and 550 cm^{-1}) or CF_3SO_3 (1250 cm^{-1}) anion and the characteristic stretching vibration of the nitrile functional group in the range 2200e2220 cm^{-1}. The coordination of the ligand to the metal center lead to a weakness of the $\nu_{N\equiv C}$ of ~-20 cm^{-1} for compounds 1-4 being this value somehow higher (-47 cm^{-1}) for compound 5, probably due to the presence of the second nitrile acceptor group. These negative shifts observed on $\nu_{N\equiv C}$ are in good agreement with the values found before for other related η^5-monocyclopentadieny iron compounds [35-37] and show an enhanced π-backdonation from the metal *d* orbitals to the π* orbital of the N≡C group leading to a decreased N≡C bond order.

^{1}H NMR chemical shifts of the cyclopentadienyl ring are displayed in the characteristic range of monocationic iron(II) complexes (4.70-4.90 ppm, Table 1). The effect of coordination on the nitrile ligands is observed through the shielding of the *ortho* protons relatively to N≡C coordination position (≈1.20 ppm) in compounds 2-4 indicating an electronic flow towards the heteroaromatic ligand due to π-backdonation involving the metal center. Furthermore, an increased electronic density was also found in compound 1 in both ortho (≈0.30 ppm) and *meta* (≈1.20 ppm) protons with special relevance for the meta position (opposite to N in the heteroaroamtic ring) probably due to a higher contribution of the corresponding resonance form. The electronic flow in compound 1 is still observed in the second fused ring (≈0.20 ppm). This shielding effect on the second fused ring was also observed for compounds 2 and 3. Here, the difference in the anion did not cause any additional effect. Relatively to the pyrazinecarbonitrile complexes (4 and 5) both protons suffered a shielding of about 0.30 ppm. ^{13}C NMR data confirm the evidence found for proton spectra. The Cp ring chemical shifts are in the range usually observed for Fe(II) cationic derivatives, a significant deshielding (up to ≈14 ppm) being observed on the carbon of the N≡C functional group upon coordination. All the other carbons of the chromophore ligand were only slightly deshielded or remained almost unchanged for the studied compounds. ^{31}P NMR data of the complexes showed the typical septuplet of the PF_6 anion at approximately - 144 ppm (with the exception of compound 3 where the PF_6 anion was replaced by CF_3SO_3). Moreover, a single sharp signal corresponding to the phosphine coligand (≈96 ppm) was observed for all the complexes, revealing the equivalency of the two phosphorus atoms, together with the expected deshielding upon coordination, in accordance with its σ donor character. Table 1 displays the ^{1}H NMR chemical shifts of the ligands (L1-L4) and corresponding complexes (1-5) in $(CD_3)_2CO$.

3.2. UV-Vis studies

The optical absorption spectra of these five new Fe(II) complexes and all the ligands were recorded in 10^{-3}-10^{-5}M dichloromethane solutions in order to identify any MLCT absorption and π-π* absorption bands expected for these complexes (Table 2). The electronic spectra of all the compounds showed intense absorption bands in the UV region, which can be assigned to electronic transitions occurring both in the organometallic fragment $\{FeCp(dppe)\}^+$ (λ ≈ 235-260 nm) and in the coordinated chromophore (λ ≈ 260-450 nm) (Fig. 1). Additional charge transfer (CT) bands were also observed in all studied complexes. In fact, all complexes presented one band compatible with a MLCT nature, which was confirmed by solvatochromism studies in DMSO (example given in Fig. 2 for complex 1).

3.3. X-ray structural studies of the complexes [Fe(η^5-C$_5$H$_5$)(dppe)(2-cq)][PF$_6$] 1 and [Fe(η^5-C$_5$H$_5$)(dppe)(3-cq)][CF$_3$SO$_3$] 3

Suitable crystals for X-ray diffraction studies of the complexes [Fe(η^5-C_5H_5)(dppe)(2-cq)][PF_6] 1 and [Fe(η^5-C_5H_5)(dppe)(3-cq)] [CF_3SO_3] 3, crystallized in different crystalline systems and space groups (monoclinic $P2_1/c$ and monoclinic $P2_{1/n}$ space groups, respectively). Crystal data and structure refinement for both complexes are collected in Table 3. In Fig. 3 and Fig. 4 the molecular structure of both complexes 1 and 3 are respectively presented. Both complexes present the usual distorted three-legged piano stool geometry for η^5-monocyclopentadienyl complexes confirmed by P-Fe-P angles of 86.93e87.11° and N-Fe-P angles varying from 90.02 to 92.64°, with the remaining η^5-Cp(centroid)-Fe-X (with X = N or P) angles between 120.40 and 128.39° (see Table 4). These values are within the range found for η^5-monocyclopentadienylmetal nitrile derivatives with coordinated phosphanes. [38-40] The distances Fe-η^5-Cp(centroid) are very similar in both complexes (1.7153 Å for complex 1, and 1.7164 Å for complex 3) and in good agreement with the donor/acceptor nature and number of other ligands bound to iron atom. The distances Fe-N≡C range from 1.8670 to 1.8865Å are well within the values expected for this family of compounds and their bond angles present only a slight deviation of the linearity, with values in accordance to those found for related compounds [38-40]. Different spatial orientation of the two isomeric ligands in both complexes can be observed. This fact can have some biological importance since it might determine the way of interaction of each complex with DNA or other biological molecules. In Table 4, the main bond lengths and angles are presented.

3.4. Electrochemical studies

In order to obtain an insight on the electron richness of the organometallic fragment and on the coordinated ligands, the electrochemical properties of the ligands L1-L4 and the new iron(II) complexes were studied by cyclic voltammetry in acetonitrile and dichloromethane solutions (1 x 10^{-3} M) using 0.1 M or 0.2 M tetrabutylammonium hexafluorophosphate ($TBAPF_6$) as supporting electrolyte, between the limits imposed by the solvents. The electrochemical data measured for the studied compounds at the scan rate of 0.200 V/s, are reported in Table 5 and Table 6. The redox behavior of the ligands L1-L3 was characterized by an irreversible reductive process near -1.70 V, whereas for the 2,3-pyrazinedicarbonitrile ligand (L4) this process is observed at ~-1.15 V, for both solvents. The electrochemical responses of the iron(II) compounds 1, 2, 4 and 5 in acetonitrile were characterized by the presence of an irreversible redox process in the positive potential range and two or three reductive processes at negative potentials. This behavior is also expected for compound 3 since its cation is isostructural of compound 2. The cyclic voltammogram of complex [FeCp(dppe)(2,3-dcpz)][PF_6] 5 is

showed on Fig. 5 and typifies the behavior found for all the complexes in this solvent. The irreversible oxidation placed in the range 0.80e0.92 V can be attributed to the metal centered process (Fe^{II}/Fe^{III}). The correspondent reductive wave was observed at 0.62 V for all the complexes and no changes in this potential were observed at different scan rates. This behavior can be related with an $Fe^{II} \rightarrow Fe^{III}$ oxidation, leading to the 17-electron species $[FeCp(dppe)(L)]^{2+}$, formed on the electrode surface which undergo fast substitution of the cyanoquinoline or pyrazine ligands by an acetonitrile molecule. The formed $[FeCp(dppe)(NCCH_3)]^{+}$ species is responsible for the observed reductive process when the scan direction is reverted. Moreover, the presence of a small reductive wave in the free ligand position (Epc = -.16 V) (Fig. 5) confirms the ligand exchange process. This result is consistent with the redox behavior of the isolated complex $[FeCp(dppe)(NCCH_3)][PF_6]$ (Fig. 5) studied before in an independent experiment for related monocyclopentadienyliron(II)dppe derivatives [39] where the same electrochemical ligand exchange process was observed. In fact, for complexes $[FeCp(dppe)(NC\{SC_4H_2\}_nNO_2)][PF_6]$, the substitution of the thiophene ligands by the acetonitrile solvent was observed during the oxidative process in the electrochemical experiments. The reductive processes found at negative potentials were attributed to ligand-based processes occurring at the coordinated cyanoquinoline (L1 and L2) or pyrazine (L4) ligands, which became easier upon coordination.

The electrochemical response of compounds 1, 2 and 4 in dichloromethane is slightly different. Fig. 6 shows the cyclic voltammogram of complex $[Fe(\eta^5\text{-}C_5H_5)(dppe)(3\text{-}cq)][PF_6]$ 2 which typifies the electrochemical behavior of complexes 1 and 2 with the cyanoquinoline ligands. No substitution processes involving solvent molecules were observed and the redox behavior is characterized by the presence of a single quasi-reversible process (I) attributed to the Fe^{II}/Fe^{III} redox pair in the range 0.84-0.90 V at positive potentials and one or two irreversible reductive waves at negative range (II and III, see Fig. 6) derived from processes occurring at the coordinated cyanoquinoline ligands. Nevertheless, for complex 4 a distinct behavior was observed and only an irreversible metal centered oxidation at 0.66 V was observed, indicating a complete decomposition process for the complex after iron(II) oxidation. Moreover, the instability in the electrochemical cell of compound 5 did not allow further studies.

3.5.1. Atomic force microscopy

Compounds 1e5 were incubated for 4 h at 37 °C in the molar relationship compound:DNA = 1:2. The images obtained by AFM are presented in Fig. 7. These images show that all the compounds modify the free DNA forms. In Fig. 7(a) the free pBR322 plasmid DNA shows the usual open and supercoiled forms. The image (b) shows the modifications caused by compound 1 after incubation with pBR322 DNA clearly showing broken chains and a strong interaction of the complex on DNA. In image (c) it can be mainly observed an aggregation of the forms on the mica surface and modifications in the supercoling caused by interaction of compound 2 on pBR322 DNA. Compounds 3 and 4 produce similar effects on DNA (images (d) and (e), respectively): the number of supercoiled forms deposited on the mica has increased. Finally, image (f) reveals that complex 5 causes strong supercoling in some DNA forms and kinks in those forms that remain open. The authors have observed similar effects in compounds with planar ligands which probably intercalate on DNA [41].

3.5.2. Cytotoxicity of the iron complexes against HL-60 cells

The cytotoxic effect of the iron complexes was examined on human leukemia cancer cells (HL-60) using the MTT assay, a colorimetric determination of cell viability during in vitro treatment with a drug. The assay, developed as an initial stage of drug screening, measures the amount of MTT reduction by

455 mitochondrial dehydrogenase and assumes that cell viability (corresponding to the reductive activity) is
456 proportional to the production of purple formazan that is measured spectrophotometrically. A low IC_{50}
457 is desired and implies cytotoxicity or antiproliferation at low drug concentrations. All the new Fe(II)
458 complexes were tested, together with cisplatin (CDDP) as a positive control. Cells were exposed to each
459 compound continuously for a 24 h or a 72 h period of time and then assayed for growth using the MTT
460 endpoint assay. Table 7 presents the IC_{50} values against HL-60 cells. The IC_{50} values at 24 h are lower
461 than that for the reference drug, cisplatin. At 72 h, compounds 2 and 4 show higher IC_{50} values than
462 cisplatin, although compounds 1, 3 and 5 present an excellent antiproliferative behavior with IC_{50} values
463 lower than cisplatin forecasting interesting structureeactivity relationships.

464

465 *3.6. Quantification of apoptosis by Annexin V binding and flow cytometry*

466 We have also analyzed, by Annexin V-PI flow cytometry, whether complexes 1-5 are able to induce
467 apoptosis in HL-60 cells after 24 h of incubation at equitoxic concentrations (IC_{50} values). Annexin V
468 binds phosphatidyl serine residues, which are asymmetrically distributed towards the inner plasma
469 membrane but migrate to the outer plasma membrane during apoptosis [33]. As it can be seen in Table
470 8, complex 3 is able to induce apoptosis death in a 26.21%, close to that of cisplatin. Compounds 1, 4
471 and 5, induce cell death by apoptosis in a lower percentage. Complex 2 presents only a discrete
472 percentage of apoptosis at IC_{50} dose, being the major death process caused by necrosis.

473

4. Conclusions

A new family of five half sandwich compounds derived from "$Fe^{II}(\eta_5\text{-}C_5H_5)$" bearing a coordinated nitrile ligand, which structure comprises one or two N-heteroaromatic rings, has been synthesized and successfully characterized. Spectroscopic evidence shows a strong p-backdonation involving the metal center. X-ray studies for two of these new compounds revealed crystallization in the monoclinic $P2_{1/c}$ and monoclinic $P2_{1/n}$ space groups.

In a preliminary approach to evaluate the cytotoxic behavior of these new compounds against cancer cells, some studies were carried out involving human leukemia cancer cells (HL-60) by MTT assay. Also their interaction AFM images with pBR322 DNA plasmid show different behaviors that can be related with the NCL ligand. Indeed, IC_{50} values together with the apoptosis results show significant differences between the whole series of compounds. There are some main conclusions that can be drawn: i) compound 1, bearing the 2-quinolinecarbonitrile, presents the best cytotoxicity and its AFM image showed the most relevant modifications in pBR322 DNA; ii) structural difference in the position of the nitrile group in compounds 1 and 2 (ortho vs. meta) leads to a decrease on the cytotoxicity (4-fold); iii) comparison of results of compounds 2 and 3 (bearing in both cases the 3-quinolinecarbonitrile ligand) shows that the replacement of PF_6 by CF_3SO_3 leads to a more cytotoxicity compound and the principal mechanism of death is changed from necrosis to apoptosis; iv) 2-pyrazinecarbonitrile (L3) leads to the less cytotoxic compound (4); and finally v) the introduction of a second nitrile group in L3 leads to a 3-fold increase in the cytotoxic behavior (compound 5). The overall results show that after 24 h of incubation all the compounds are more cytotoxic than cisplatin. Thus, this is a potentially interesting family of compounds to be studied in the frame of anticancer drugs.

497 **ACKNOWLEDGEMENTS**

498

499 The authors thank financial support from the Portuguese Foundation for Science and Technology for
500 the projects PEst-OE/QUI/UI0536/2011, PTDC/QUI-QUI/118077/2010, PTDC/QUI-
501 QUI/101187/2008 and SFRH/BPD/80459/2011 (Andreia Valente's postdoctoral scholarship) and
502 Spanish Ministry of Ciencia e Innovacion, projects CTQ2008-02064 and BIO2010-22321-C02-01.

503

504 **References**

505

506 [1] H. Köpf, P. Köpf-Maier, Angew. Chem. 91 (1979) 509.

507 [2] T.M. Klapötke, H. Köpf, I.C. Tornieporth-Oetting, P.S. White, Organometallics 13 (1994)
508 3628e3633.

509 [3] C.V. Christodoulou, A. Eliopoulos, A. Young, L. Hodgkins, D.R. Ferry, D.J. Kerr, Br. J. Cancer
510 77 (1998) 2088e2097.

511 [4] P. Köpf-Maier, Anticancer Res. 19 (1999) 493e504.

512 [5] K. Kröer, U.R. Kleeberg, K. Mross, L. Edler, D.K. Hossfeld, Onkologie 23 (2000) 60e62.

513 [6] K. Mross, P. Robben-Bathe, L. Edler, J. Baumgart, W.E. Berdel, H. Fiebig, C. Unger, Onkologie
514 23 (2000) 576e579.

515 [7] L.V. Popova, V.N. Babin, Y.A. Belousov, Y.S. Nekrasov, A.E. Snegireva, N.P. Borodina, G.M.
516 Shaposhnikova, O.B. Bychenko, P.M. Raevskii, Appl. Organometal. Chem. 7 (1993) 85e94.

517 [8] P. Köpf-Maier, H. Köpf, E.W. Neuse, J. Cancer Res. Clin. Oncol. 108 (1984) 336e 340.

518 [9] W. Henderson, S.R. Alley, Inorg. Chim. Acta 322 (2001) 106e112.

519 [10] P. Köpf-Maier, H. Köpf, Chem. Rev. 87 (1987) 1137e1152.

520 [11] G. Gasser, I. Ott, N. Metzler-Nolte, J. Med. Chem. 54 (2011) 3e25.

521 [12] R.E. Morris, R.E. Aird, P.D.S. Murdoch, H. Chen, J. Cummings, N.D. Hughes, S. Parsons, A.
522 Parkin, G. Boyd, D. Jodrell, P.J. Sadler, J. Med. Chem. 44 (2001) 3616e3621.

523 [13] R.E. Aird, J. Cummings, M. Muir, R.E. Morris, H. Chen, P.J. Sadler, Br. J. Cancer 86 (2002)
524 1652e1657.

525 [14] S.J. Dougan, M. Melchart, A. Habtermariam, S. Parsons, P.J. Sadler, Inorg. Chem. 45 (2006)
526 10882e10894.

527 [15] F. Wang, J. Bella, J.A. Parkinson, P.J. Sadler, J. Biol. Inorg. Chem. 10 (2005) 147e 155.

528 [16] H. Chen, J.A. Parkinson, O. Novakova, J. Bella, F. Wang, A. Dawson, R. Gould, S. Parsons, V.
529 Brabec, P.J. Sadler, Proc. Natl. Acad. Sci. 100 (2003) 14623e 14628.

530 [17] V. Marini, P. Christofis, O. Novakova, J. Kasparkova, N. Farrell, V. Brabec, Nucleic Acids Res.
531 33 (2005) 5819e5828.

532 [18] C. Scolaro, A. Bergamo, L. Brescacin, R. Delfino, M. Cocchietto, G. Laurenczy, T.J. Geldbach,
533 G. Sava, P.J. Dyson, J. Med. Chem. 48 (2005) 4161e4171.

534 [19] M.H. Garcia, T.S. Morais, P. Florindo, M.F.M. Piedade, V. Moreno, C. Ciudad, V. Noe, J. Inorg.
535 Biochem. 103 (2009) 354.

536 [20] V. Moreno, J. Lorenzo, F.X. Aviles, M.H. Garcia, J. Ribeiro, T.S. Morais, P. Florindo, M.P.
537 Robalo, Bioinorg. Chem. Appl. (2010), 11, Article ID 936834.

538 [21] V. Moreno, M. Font-Bardia, T. Calvet, J. Lorenzo, F.X. Avilés, M.H. Garcia, T.S. Morais, A.
539 Valente, M.P. Robalo, J. Inorg. Biochem. 105 (2011) 241.

[22] T.S. Morais, T.J.L. Silva, F. Marques, M.P. Robalo, F. Avecilla, P.J.A. Madeira, P.J.G. Mendes, I. Santos, M.H. Garcia, J. Inorg. Biochem. 114 (2012) 65e74.

[23] A.I. Tomaz, T. Jakusch, T.S. Morais, F. Marques, R.F. de Almeida, F. Mendes, E.A. Enyedy, I. Santos, J.C. Pessoa, T. Kiss, M.H. Garcia, J. Inorg. Biochem. 117 (2012) 261e269.

[24] T.S. Morais, F. Santos, L. Côrte-Real, F. Marques, M.P. Robalo, P.J.A. Madeira, M.H. Garcia, J. Inorg. Biochem. 122 (2013) 8e17.

[25] A.R. Timerbaev, C.G. Hartinger, S.S. Aleksenko, B.K. Keppler, Chem. Rev. 106 (2006) 2224e2248.

[26] A.C. Gonçalves, T.S. Morais, M.P. Robalo, F. Marques, F. Avecilla, C.P. Matos, I. Santos, A.I. Tomaz, M.H. Garcia, J. Inorg. Biochem. 129 (2013) 1e8.

[27] D.D. Perrin, W.L.F. Amarego, D.R. Perrin, Purification of Laboratory Chemicals second ed., Pergamon, New York, 1980, pp. 65e371.

[28] M.L.H. Green, R. Whiteley, J. Chem. Soc. A (1971) 1943.

[29] G.M. Sheldrick, A Program for Automatic Solution of Crystal Structure, Univer Goettingen, Germany, 1997.

[30] G.M. Sheldrick, A Program for Crystal Structure Refinement, Univer Goettingen, Germany, 1994.

[31] International Tables of X-Ray Crystallography, vol. IV, Kynoch Press, 1974, pp. 99e100 and 149.

[32] N.G. Conelly, W.E. Geiger, Chem. Rev. 96 (1996) 877e910.

[33] I. Vermes, C. Haanen, H. Steffens-Nakken, C. Reutelingsperger, J. Immunol. Meth. 184 (1995) 39e51.

[34] G.S. Ashby, M.I. Bruce, I.B. Tomkins, R.C. Walli, Aust. J. Chem. 32 (1979) 1003e 1016.

[35] M.H. Garcia, P. Florindo, M.F.M. Piedade, M.T. Duarte, M.P. Robalo, J. Heck, C. Wittenburg, J. Holtmann, E. Licandro, J. Organomet. Chem. 693 (2008) 2987e2999.

[36] A.R. Dias, M.H. Garcia, J.C. Rodrigues, M.L.H. Green, K.K. Lai, S.M. Klueber, J. Organomet. Chem. 475 (1994) 241.

[37] A. Valente, S. Royer, M. Narendra, T.J.L. Silva, P.J.G. Mendes, M.P. Robalo, M. Abreu, J. Heck, M.H. Garcia, J. Organomet. Chem. 736 (2013) 42e49.

[38] M.H. Garcia, M.P. Robalo, A.R. Dias, M.F.M. Piedade, A. Galvão, M.T. Duarte, W. Wenseleers, E. Goovaerts, J. Organomet. Chem. 619 (2001) 252.

[39] R.L. Cordiner, D. Albesa-Jové, R.L. Roberts, J.D. Farmer, H. Puschmann, D. Corcoran, A.E. Goeta, J.A.K. Howard, P.J. Low, J. Organomet. Chem. 690 (2005) 4908.

[40] Maria Helena Garcia, Pedro Florindo, Maria de Fátima M. Piedade, Stefano Maiorana, Emanuela Licandro, Polyhedron 28 (2009) 621e629.

[41] X. Riera, V. Moreno, C.J. Ciudad, V. Noe, M. Font-Bardia, X. Solans, Bioinorg. Chem. Appl. (2007) 1e15. Article ID 98732.

578 **Legends to figures**

579

580 **Scheme 1.** Reaction scheme for the synthesis of the new Fe(II) complexes and the ligand structures
581 numbered for NMR purposes

582

583 **Figure 1.** Electronic spectra of [FeCp(dppe)(L)]þ (1e5) in dichloromethane solutions:—1; - - - - 2; ·····3;
584 – – 4; – · – · 5.

585

586 **Figure 2.** Electronic spectra of [Fe(η^5-C_5H_5)(dppe)(2-cq)][PF_6] 1 in dichloromethane (·····) and
587 dimethylsulfoxide (—) showing solvatochromism of the MLCT transition.

588

589 **Figure 3.** ORTEP drawing of [Fe(η^5-C_5H_5)(dppe)(2-cq)][PF_6] 1 with atomic numbering scheme.

590

591 **Figure 4.** ORTEP drawing of [Fe(η^5-C_5H_5)(dppe) (3-cq)][CF_3SO_3] 3 with atomic numbering scheme.

592

593 **Figure 5.** Cyclic voltammetry of complexes [Fe(η^5-C_5H_5)(dppe) (2,3-dcpz)][PF_6] 5 (—) and [Fe(η^5-
594 C_5H_5)(dppe)(NCMe)][PF_6] (- - - - -) in acetonitrile (v = 200 mV/s).

595

596 **Figure 6.** Cyclic voltammetry of complex [Fe(η^5-C5H5)(dppe)(3-cq)][PF6] 2 (—) and 3-cq ligand (- -
597 - - -) in dichloromethane (v = 200 mV/s).

598

599 **Figure 7.** AFM images of (a) plasmid pBR322 DNA and plasmid pBR322 DNA incubated with complex
600 (b) [Fe(η^5-C_5H_5)(dppe)(2-cq)][PF_6] 1, (c) [Fe(η^5-C_5H_5)(dppe)(3-cq)][PF_6] 2, (d) [Fe(η^5-
601 C_5H_5)(dppe)(3-cq)][CF_3SO_3] 3, (e) [Fe(η^5-C_5H_5)(dppe)(cpz)][PF_6] 4 and (f) [Fe(η^5-C_5H_5)(dppe)(2,3-
602 dcpz)][PF_6] 5.

603

604

605 **Table 1.** ^{1}H NMR data for the ligands (L1eL4) and the complexes (1e5), in $(CD_3)_2CO$.

606

	H_3	H_4	H_5	H_6	H_7	H_8	H_9	H_{10}	Cp
L1	–	8.13	7.93	7.81	8.13	–	7.95	8.63	–
1	–	7.96	7.73	7.88	7.96	–	6.78	8.30	4.75
L2	9.11	–	8.14	7.78	7.98	8.11	–	8.92	–
2	7.92	–	8.00	7.71	7.92	7.85	–	7.68	4.73
3	7.92	–	8.01	7.71	7.92	7.87	–	7.71	4.74
L3	9.13	8.95	8.84	–	–	–	–	–	–
4	7.88	8.67	8.55	–	–	–	–	–	4.75
L4	–	9.14	9.14	–	–	–	–	–	–
5	–	8.83	8.82	–	–	–	–	–	4.86

607

608

609

610

611 **Table 2.** Optical spectra data for complexes $[Fe(\eta^5\text{-}C_5H_5)(dppe)(L)]^+$ (1-5) in dichloromethane and
612 dimethylsulfoxide solutions. Sh: shoulder.

613

Compound	λ_{max} (nm) (ε M^{-1} cm^{-1})	
	CH_2Cl_2	DMSO
$[Fe(\eta^5\text{-}C_5H_5)(dppe)(2\text{-cq})][PF_6]$ **1**	240 (73,195)	–
	385 (6049)	392 (*Sh*)
	441 (6893)	455 (7669)
$[Fe(\eta^5\text{-}C_5H_5)(dppe)(3\text{-cq})][PF_6]$ **2**	239 (75,639)	–
	275 (*Sh*)	–
	376 (7169)	386 (6559)
	429 (5136)	442 (7292)
$[Fe(\eta^5\text{-}C_5H_5)(dppe)(3\text{-cq})][CF_3SO_3]$ **3**	239 (51,562)	–
	278 (*Sh*)	–
	369 (3559)	386 (4380)
	428 (2371)	442 (4798)
$[Fe(\eta^5\text{-}C_5H_5)(dppe)(cpz)][PF_6]$ **4**	264 (20,282)	–
	388 (*Sh*)	–
	445 (2895)	446 (5225)
$[Fe(\eta^5\text{-}C_5H_5)(dppe)(2,3\text{-cpz})][PF_6]$ **5**	266 (12,201)	–
	521 (2521)	512 (5710)

614

615

616

617

618 **Table 3** Crystal data and structure refinement for [Fe(η^5-C_5H_5)(dppe)(2-cq)][PF_6] 1 and [Fe(η^5-
619 C_5H_5)(dppe)(3-cq)][CF_3SO_3] 3.

620

Empirical formula	C_{41} H_{35} F_6 Fe N_2 P_3	C_{42} H_{35} F_3 Fe N_2 O_3 P_2 S
Formula weight	818.47	822.57
T (K)	293(2)	293(2)
Wavelength	0.71073 Å	0.71073 Å
Crystal system	Monoclinic	Monoclinic
Space group	$P2_1/n$	$P2_1/c$
a (Å)	15.927(6)	$a = 10.962(5)$
b (Å)	11.251(4)	$b = 17.000(6)$
c (Å)	21.013(3)	$c = 20.986(7)$
α (°)	90	90
β (°)	95.32(2)	$\beta = 102.57(2)$
γ (°)	90	90
V (Å^3)	3749(2)	3817(3)
Z	4	4
D_c (Mg/m^3)	1.450	1.431
Absorption coefficient (mm^{-1})	0.593	0.591
F(000)	1680	1696
Theta range for data collection (°)	1.54–28.39	2.59–32.32
Limiting indices	$-18 \le h \le 19$, $-12 \le k \le 13$, $-25 \le l \le 26$	$-13 \le h \le 15$, $-23 \le k \le 23$, $-27 \le l \le 28$
Reflections collected/unique	20,388/7170 [R(int) = 0.0265]	29,982/9989 [R(int) = 0.0387]
Completeness to theta = 25.00 (°)	93.0%	98.4%
Absorption correction	Empirical	Empirical
Max. and min. transmission	0.94 and 0.93	0.94 and 0.93
Refinement method	Full-matrix least-squares on F^2	Full-matrix least-squares on F^2
Data/restraints/ parameters	7170/49/514	9989/53/646
Goodness-of-fit on F^2	1.062	1.149
Final R indices [I > 2(I)]	$R1 = 0.0498$, $wR2 = 0.1520$	$R1 = 0.0419$, $wR2 = 0.1062$
R indices (all data)	$R1 = 0.0499$, $wR2 = 0.1521$	$R1 = 0.0446$, $wR2 = 0.1086$
Largest diff. peak/hole (e Å^3)	0.517 and −1.720	0.576 and −0.339

621

622

623

624

625 **Table 4** Selected bond lenghts and torsion angles for [Fe(η^5-C_5H_5)(dppe)(2-cq)][PF_6] 1 and [Fe(η^5-
626 C_5H_5)(dppe)(3-cq)][CF_3SO_3] 3.

627

Compound **1**		Compound **3**	
Bond lenght (Å)			
Fe–P1	2.2263(9)	2.2226(7)	Fe–P1
Fe–P2	2.2211(9)	2.2148(8)	Fe–P2
Fe–N1	1.8670(2)	1.8865(14)	Fe–N2
Fe–Cp	1.7153(17)	1.7164(12)	Fe–Cp
Angles (°)			
N(1)–Fe–C(1)	91.01(12)	127.03(7)	N(2)–Fe–C(11)
N(1)–Fe–C(5)	91.95(12)	155.73(6)	N(2)–Fe–C(15)
N(1)–Fe–C(2)	123.44(13)	92.08(8)	N(2)–Fe–C(12)
N(1)–Fe–C(3)	155.94(11)	89.59(7)	N(2)–Fe–C(13)
N(1)–Fe–C(4)	125.74(12)	121.96(7)	N(2)–Fe–C(14)
N(1)–Fe–P(2)	90.02(8)	90.07(5)	N(2)–Fe–P(2)
N(1)–Fe–P(1)	91.76(7)	92.64(5)	N(2)–Fe–P(1)
P(2)–Fe–P(1)	87.11(3)	86.93(3)	P(2)–Fe–P(1)
Cp–Fe–N(1)	120.79	120.40	Cp–Fe–N(2)
Cp–Fe–P(1)	128.39	128.39	Cp–Fe–P(1)
Cp–Fe–P(2)	127.28	127.28	Cp–Fe–P(2)

628

629

630 **Table 5.** Electrochemical data for complexes [Fe(η^5-C_5H_5)(dppe)L][PF_6] (1 -5) in acetonitrile at scan
631 rate of 200 mV s^{-1}.

632

	E_{pa} (V)	E_{pc} (V)	$E_{1/2}$ (V)	$E_{pa} - E_{pc}$ (mV)	I_c/I_a
L1	–	–1.76	–	–	–
L2	–	–1.75	–	–	–
L3	–	–1.67	–	–	–
L4	–	–1.16	–	–	–
1	0.81	–	–	–	–
	–	0.62	–	–	–
	–	–1.42	–	–	–
	–1.60	–1.69	–1.65	90	0.9
2	0.80	–	–	–	–
	–	0.62	–	–	–
	–	–1.45	–	–	–
	–	–1.70	–	–	–
4	0.89	–	–	–	–
	–	0.62	–	–	–
	–	–1.36	–	–	–
	–	–1.67	–	–	–
5	0.92	–	–	–	–
	–	0.62	–	–	–
	–	–1.07	–	–	–
	–	–1.16	–	–	–
	–	–1.70	–	–	–

633

634

635 **Table 6.** Electrochemical data for complexes [Fe(η^5-C_5H_5)(dppe)L][PF_6] (1e6) in dichloromethane at
636 scan rate of 200 mV s^{-1}.

	E_{pa} (V)	E_{pc} (V)	$E_{1/2}$ (V)	$E_{pa} - E_{pc}$ (mV)	I_c/I_a
L1	–	−1.68	–	–	–
L2	–	−1.70	–	–	–
L3	–	–	–	–	–
1	0.95	0.84	0.90	110	1.0
	–	−1.43	–	–	–
2	0.88	0.81	0.84	75	1.0
	–	−1.45	–	–	–
	–	−1.71	–	–	–
4	0.66	0.44	–	–	–

637
638
639
640
641
642

643 **Table 7.** IC50 values of iron compounds (1e5) and cisplatin against HL-60 cells.

Complex	IC_{50} (μM) 24 h	IC_{50} (μM) 72 h
[FeCp(dppe)(2-cq)][PF_6] **1**	2.73 ± 1.85	0.77 ± 0.22
[FeCp(dppe)(3-cq)][PF_6] **2**	3.71 ± 0.23	3.13 ± 0.19
[FeCp(dppe)(3-cq)][CF_3SO_3] **3**	9.79 ± 3.11	1.01 ± 0.57
[FeCp(dppe)(cpz)][PF_6] **4**	7.92 ± 1.37	5.08 ± 0.41
[FeCp(dppe)(2,3-dcpz)][PF_6] **5**	1.97 ± 0.37	1.20 ± 0.47
CDDP	15.61 ± 1.15	2.15 ± 0.1

644

645

646

647

Table 8. Percentage of HL-60 cells in each state after treatment with complexes 1e5 at IC50 concentration for 24 h of incubation.

Treatment (IC_{50} 24 h, μM)	% vital cells (*R*1)	% apoptotic cells (*R*2)	% dead cells (*R*3)	% damaged cells (*R*4)
Control	92.44	4.78	2.59	0.19
CDDP (15.6)	60.93	33.06	4.94	1.06
1 (2.73)	71.84	19.39	8.19	0.57
2 (3.71)	62.86	9.68	28.50	1.23
3 (9.79)	62.88	26.21	9.63	1.27
4 (7.92)	67.91	12.48	18.95	0.66
5 (1.2)	69.95	15.82	13.98	0.25

653 **Scheme 1.**

654

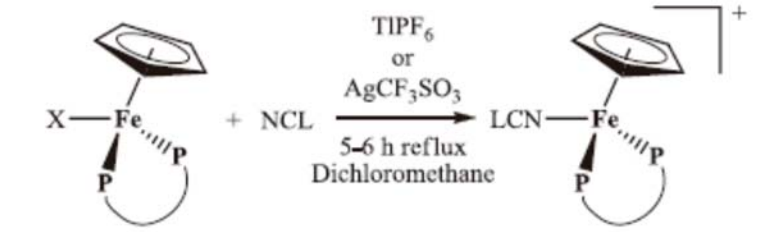

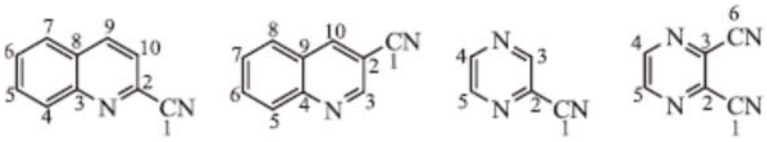

L1 (2-cq) **L2** (3-cq) **L3** (cpz) **L4** (2,3-dcpz)

Complexes:

1: L1; PF_6^-
2: L2; PF_6^-
3: L2; $CF_3SO_3^-$
4: L3; PF_6^-
5: L4; PF_6^-

655

656

657

658

659 **Figure 1**

660

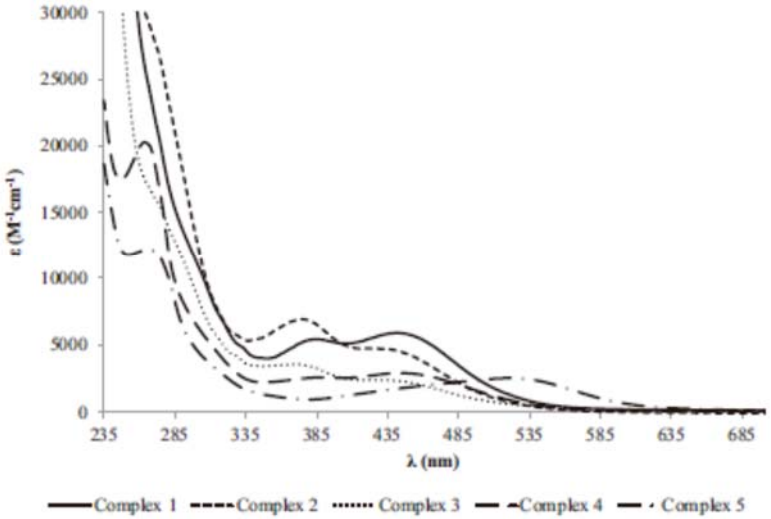

661

662

663

664

665 **Figure 2**

666

667

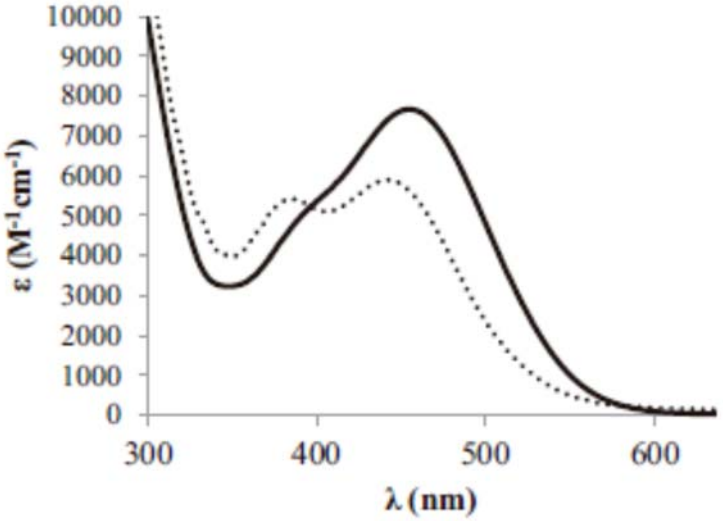

668

669

670 **Figure 3**

671

672

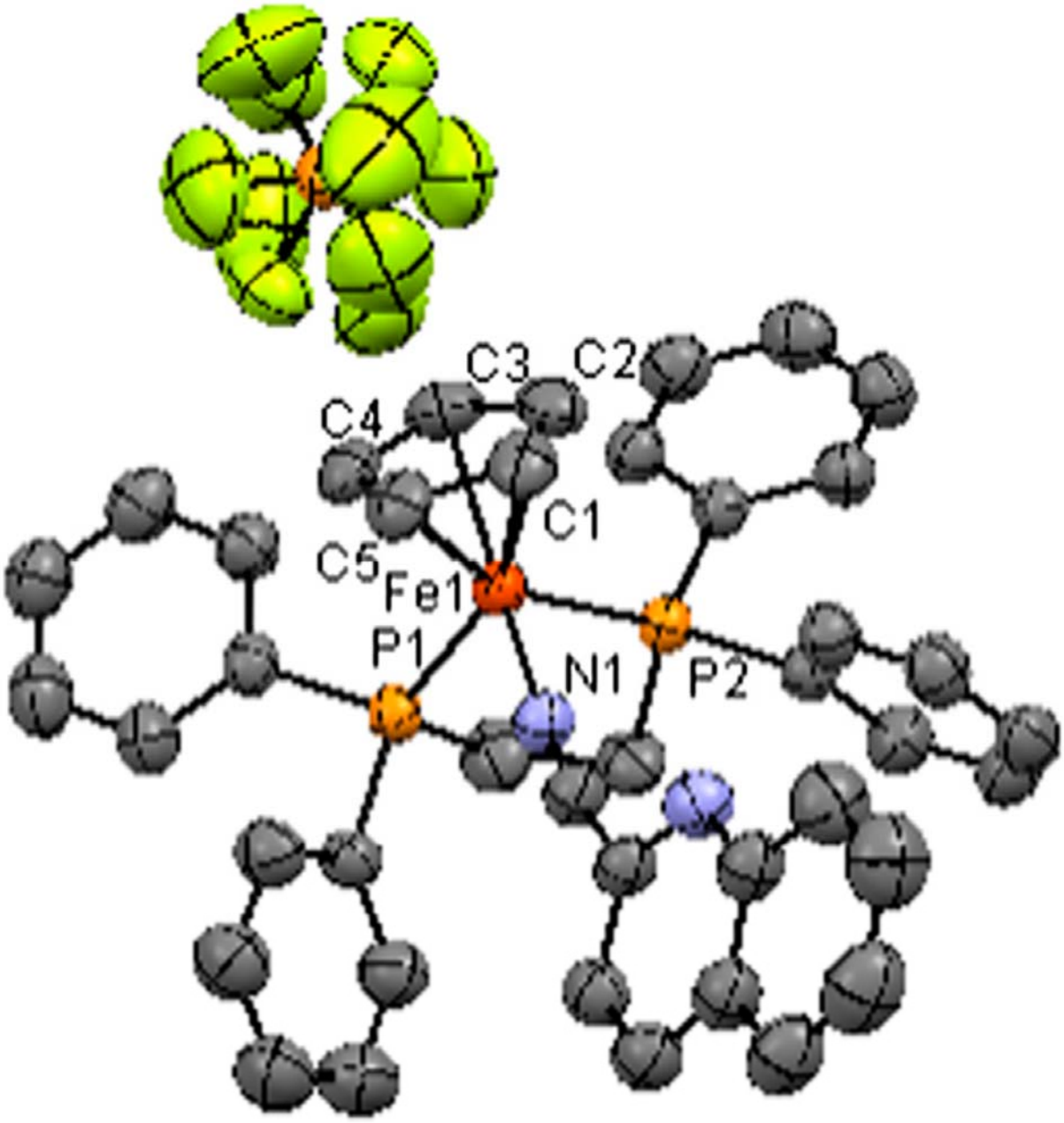

673

674

675 **Figure 4**

676

677

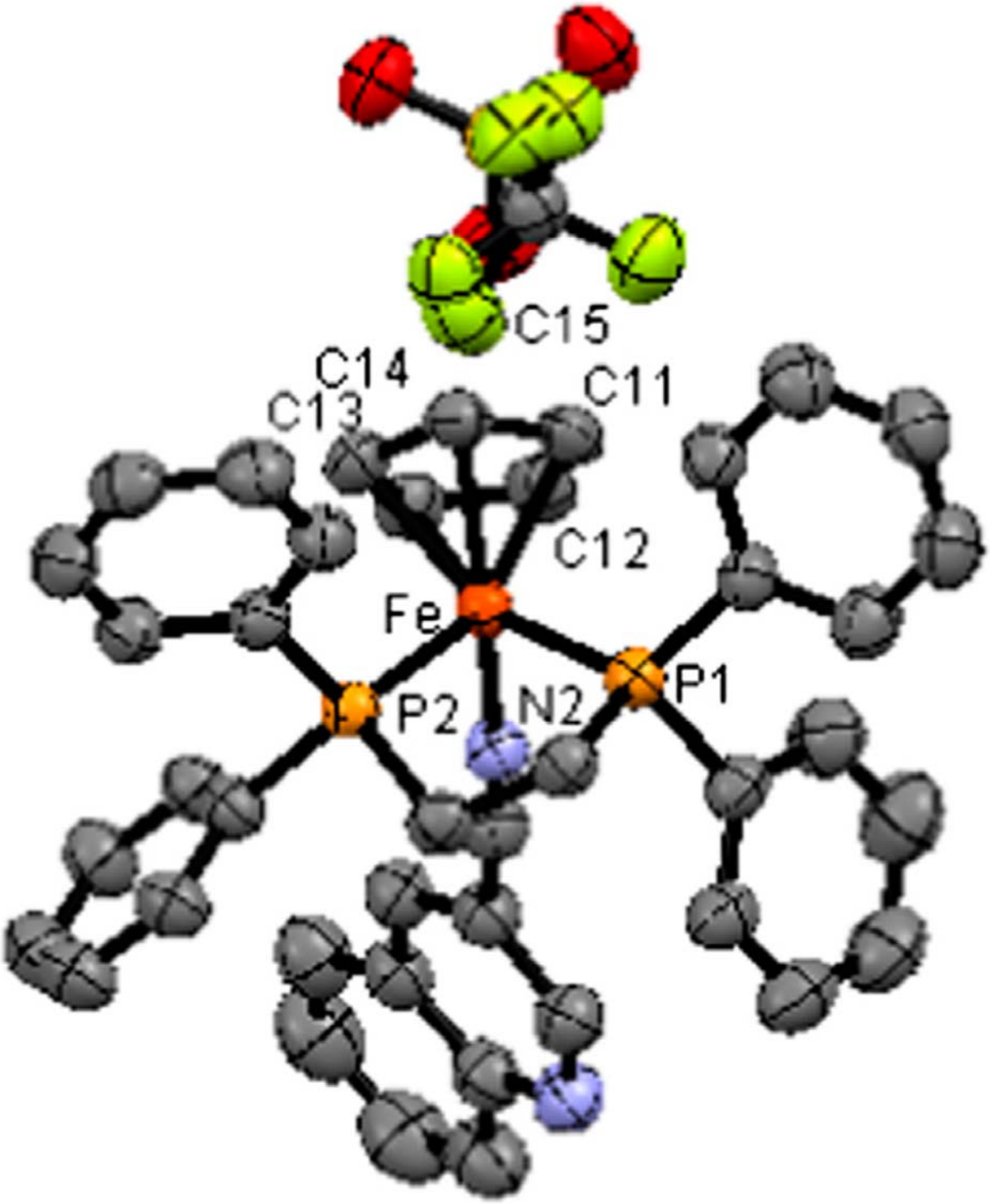

678

679

680 **Figure 5**

681

682

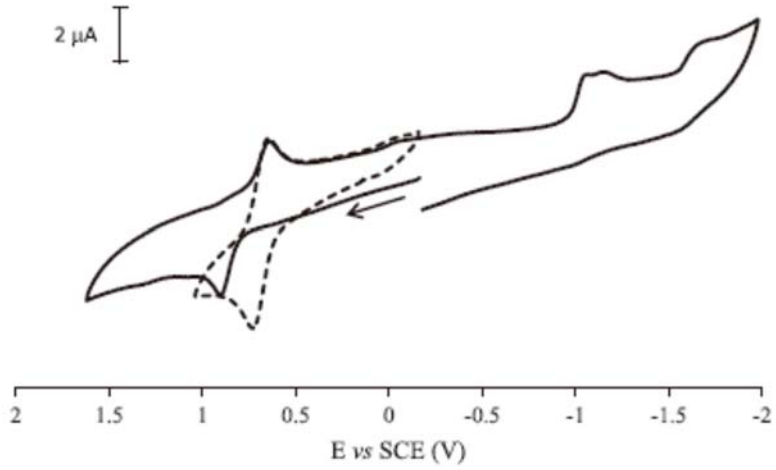

683

684

685 **Figure 6**

686

687

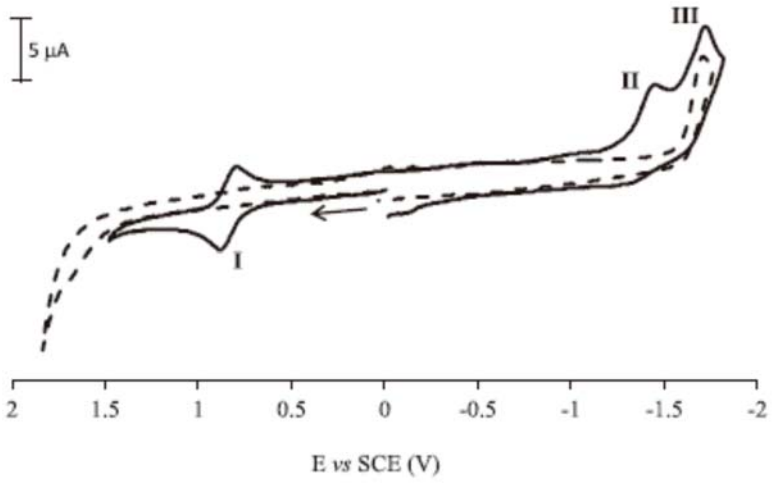

688

689

690

691 **Figure 7**

692

693

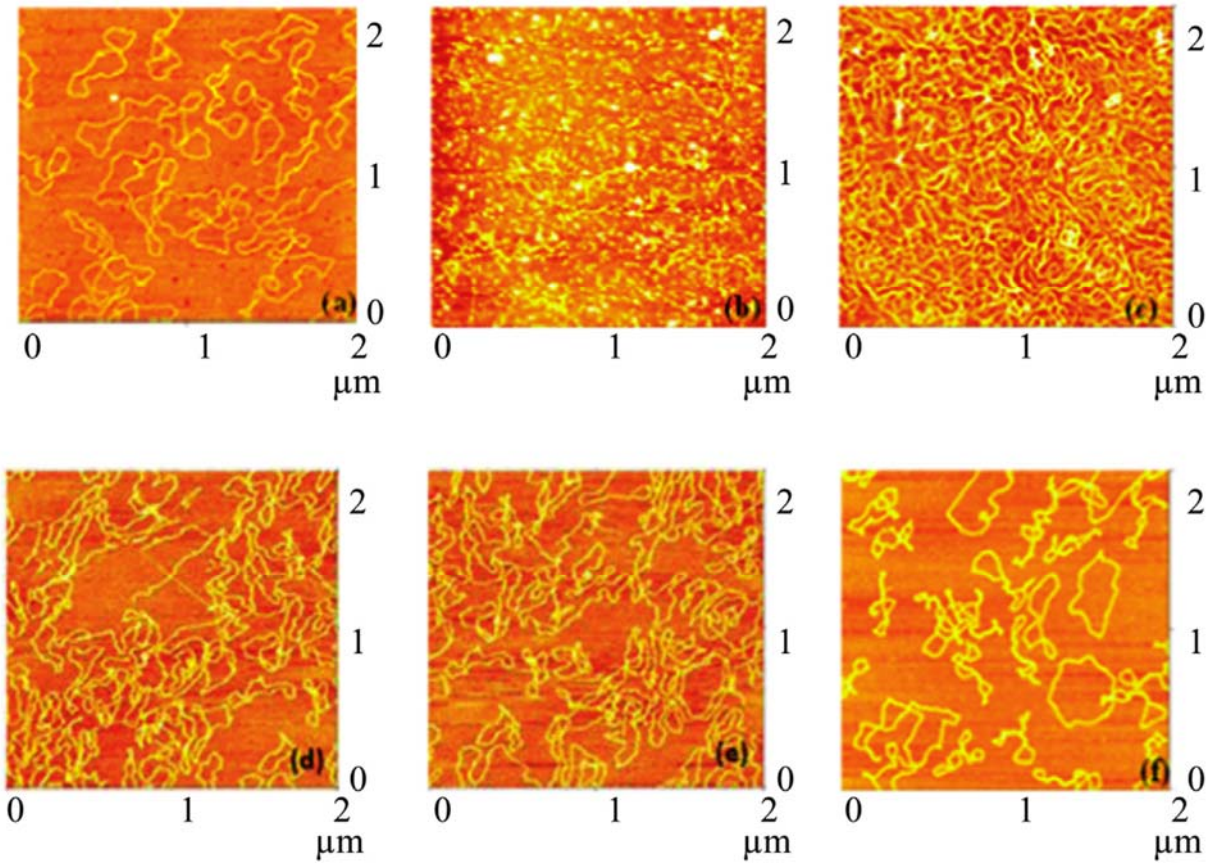

694